



THE UNIVERSITY *of* EDINBURGH

Edinburgh Research Explorer

## Low-dimensional magnetism in calcium nitridonickelate(II) $\text{Ca}_2\text{NiN}_2$

**Citation for published version:**

Kloß, SD & Attfield, P 2021, 'Low-dimensional magnetism in calcium nitridonickelate(II)  $\text{Ca}_2\text{NiN}_2$ ', *Chemical Communications*. <https://doi.org/10.1039/D1CC04001D>

**Digital Object Identifier (DOI):**

[10.1039/D1CC04001D](https://doi.org/10.1039/D1CC04001D)

**Link:**

[Link to publication record in Edinburgh Research Explorer](#)

**Document Version:**

Publisher's PDF, also known as Version of record

**Published In:**

Chemical Communications

**General rights**

Copyright for the publications made accessible via the Edinburgh Research Explorer is retained by the author(s) and / or other copyright owners and it is a condition of accessing these publications that users recognise and abide by the legal requirements associated with these rights.

**Take down policy**

The University of Edinburgh has made every reasonable effort to ensure that Edinburgh Research Explorer content complies with UK legislation. If you believe that the public display of this file breaches copyright please contact [openaccess@ed.ac.uk](mailto:openaccess@ed.ac.uk) providing details, and we will remove access to the work immediately and investigate your claim.





# Low-dimensional magnetism in calcium nitridonickelate(II) $\text{Ca}_2\text{NiN}_2^\dagger$

Simon D. Kloß \* and J. Paul Attfield \*

Cite this: DOI: 10.1039/d1cc04001d

 Received 23rd July 2021,  
 Accepted 13th September 2021

DOI: 10.1039/d1cc04001d

[rsc.li/chemcomm](http://rsc.li/chemcomm)

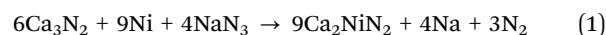
**Calcium nitridonickelate(II)  $\text{Ca}_2\text{NiN}_2$  has been prepared through a high-temperature and high-pressure azide-mediated redox reaction, demonstrating that this method can stabilise nitrides of late transition metals in relatively high oxidation states.  $\text{Ca}_2\text{NiN}_2$  crystallizes in the  $\text{Na}_2\text{HgO}_2$  structure type and displays low-dimensional antiferromagnetic ordering of  $\text{Ni}^{2+}$  spins.**

Multinary 3d transition metal nitrides have been extensively investigated with ambient and medium pressure (<1 GPa) synthesis methods for their diverse physical and electronic properties, their structural chemistry, and their close relation to the well-studied oxometallates.<sup>1–7</sup> However, access to nitrogen-rich transition metal nitrides is limited by the low energy of nitride formation<sup>8–10</sup> and especially for later transition metals such as Co, Ni and Cu, the obtainable nitrides are usually nitrogen-poor and metallic: while in molecular chemistry low-coordinate  $\text{Ni}^{\text{II}}$  imido complexes and a transient  $\text{Ni}^{\text{IV}}$  nitrido complex have been investigated,<sup>11,12</sup> currently reported solid-state nitridonickelates such as  $\text{MNiN}$  (M = Ca, Sr, Ba),  $\text{Ba}_2\text{Ni}^{2/3+}_3\text{N}_2$ , and  $\text{Li}_3\text{Sr}_3\text{Ni}^{3/4+}_4\text{N}_4$ ,<sup>13–17</sup> feature low nitrogen to metal ratios and mean Ni oxidation states of 1+ or lower.  $\text{LiNiN}$  is the only well-characterized compound with  $\text{Ni}(\text{II})$ <sup>18</sup> as a proposed  $\text{Na}_2\text{HgO}_2$ -type; the reported  $\text{Sr}_2\text{Ni}^{\text{II}}\text{N}_2$  was later shown to be a cyano-nitridonickelate(0) *i.e.*  $\text{Sr}_2[(\text{NC})\text{NiN}]$ .<sup>19,20</sup>

A higher nitrogen content could lead to opening of a band gap enabling semiconductivity, light-absorption for solar energy conversion applications, and emergence of localized-electron properties such as charge order and magnetism as found in oxo-metallates.<sup>21–25</sup> However, although recent high-throughput calculations have predicted many new nitride systems highlighting the great potential for materials discovery, employable synthesis routes for nitrogen rich compounds remain scarce.<sup>9,26</sup>

Applying high pressures in the gigapascal range is favorable for stabilizing nitrides against loss of dinitrogen but starting materials like transition metals or their binary nitrides often need to be nitrified *in situ*. This was demonstrated with  $\text{N}_2$ -loaded diamond anvil cell syntheses of binary materials such as metal diazenides and pernitrides like  $\text{NiN}_2$  or  $\text{PtN}_2$ , polynitrides like  $\text{FeN}_4$ , and pentazolate salts like  $\text{CsN}_5$ .<sup>27–30</sup> Much less work has been done in multianvil large-volume presses but recently it was discovered that sodium azide can be used as a  $\text{N}_2$  source, as demonstrated in the syntheses of rocksalt-type  $\text{Mg}_{0.4}\text{Fe}_{0.6}\text{N}$  and the highly oxidized nitridoferrate(IV)  $\text{Ca}_4\text{FeN}_4$ .<sup>31–33</sup> Large-volume-presses offer the advantage over DACs that larger sample quantities for physical properties measurements can be prepared and multinary systems can more easily be studied.

Here we adapt the azide-route for the preparation of a new  $\text{Na}_2\text{HgO}_2$ -type nitridonickelate with Ni in the 2+ state, which is very unusual in this class of materials.  $\text{Ca}_2\text{NiN}_2$  was obtained at 900 °C and 8 GPa following eqn (1) with a 10 mol% excess of  $\text{Ca}_3\text{N}_2$  as a black moisture sensitive (lifetime in air several minutes) microcrystalline powder (Fig. S1, ESI†). The excess of  $\text{Ca}_3\text{N}_2$  and  $\text{NaN}_3$  is required to suppress the formation of byproduct  $\text{CaNiN}$ , which also forms when raising the temperature or lowering the pressure.<sup>13</sup>



$\text{Ca}_2\text{NiN}_2$  was investigated with EDX spectroscopy showing a mean composition of  $\text{Ca}_{2.0(2)}\text{Ni}_{0.9(1)}\text{N}_{2.0(2)}$  (normalized on Ca, 18 datapoints averaged, Table S1, ESI†). EDX also revealed that Na is finely dispersed throughout the sample (which precluded direct measurements of sample conductivity) and was identified through powder diffraction (Fig. 1a). There was no evidence of a Ca/Na mixed position through initial Rietveld refinement, consistent with  $\text{Ca}_4\text{FeN}_4$ , where the absence of Na incorporation was verified through Mössbauer and magnetization measurements.<sup>32</sup> The excess  $\text{Ca}_3\text{N}_2$  might have formed an amorphous byproduct as the powder pattern showed a heightened background at low  $Q$ .

Centre for Science at Extreme Conditions, University of Edinburgh,  
 Edinburgh EH9 3FD, UK. E-mail: v1skloss@ed.ac.uk, j.p.attfield@ed.ac.uk

† Electronic supplementary information (ESI) available. CCDC 2096979. For ESI and crystallographic data in CIF or other electronic format see DOI: 10.1039/d1cc04001d



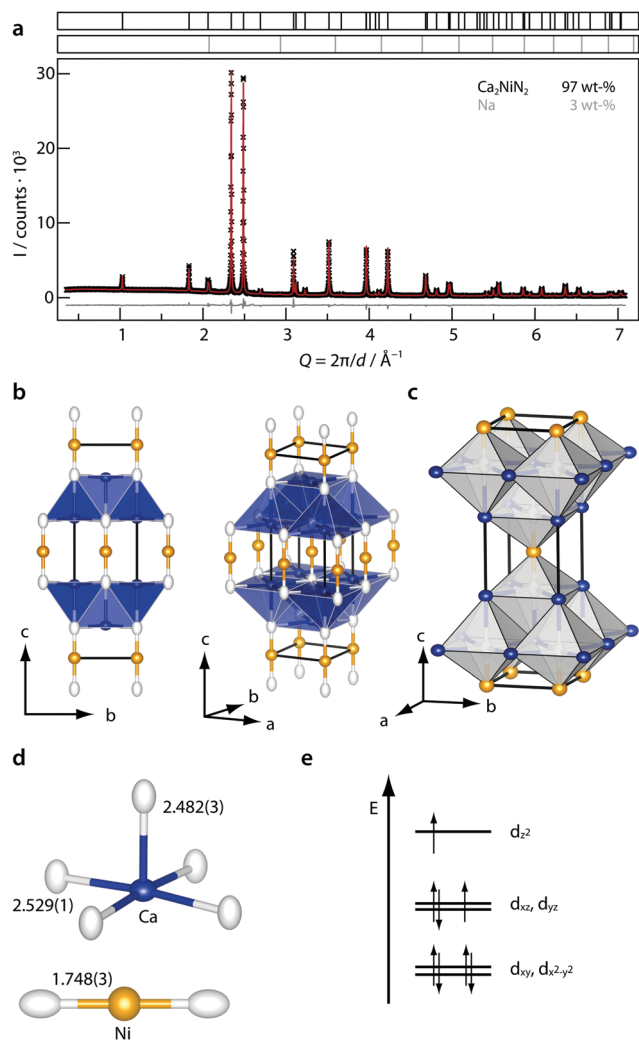


**Fig. 1** (a) Rietveld refinement of  $\text{Ca}_2\text{NiN}_2$  with datapoints as black crosses, Rietveld fit as red line, difference curve as grey line and tick marks of  $\text{Ca}_2\text{NiN}_2$  and the Na byproduct shown above. The weight percent ratio of  $\text{Ca}_2\text{NiN}_2$  and Na was refined to 97/3, which is in the range expected from stoichiometry, ideally 94/6. The diffuse background at low  $Q$ -values is probably due to amorphization of excess  $\text{Ca}_3\text{N}_2$ . (b–d) Structure of  $\text{Ca}_2\text{NiN}_2$  with Ca as blue, Ni as orange and N as white ellipsoids at a 90% probability level.  $\text{CaN}_5$  square pyramids are shown in blue and  $\text{NCa}_5\text{Ni}$  octahedra in grey. (e) Energy level diagram for  $d^8$  Ni in linear coordination and simple  $\sigma$ -bonding adapted from literature.<sup>11</sup>

The crystal structure of  $\text{Ca}_2\text{NiN}_2$  (space group  $I4/mmm$ ,  $Z = 2$ ,  $a = 3.57206(2)$ ,  $c = 12.19453(10)$  Å,  $V = 155.719(5)$  Å<sup>3</sup>) was determined from powder diffraction data by charge flipping in  $P4n2$  and subsequent refinement (Fig. 1a) in  $I4/mmm$ . Details and results of the refinement are in Tables S2 and S3 (ESI†).

$\text{Ca}_2\text{NiN}_2$  crystallizes in the  $\text{Na}_2\text{HgO}_2$ -structure type and features linear  $[\text{Ni}^{\text{II}}\text{N}_2]^{4-}$  complex anions as well as layers of edge-sharing quadratic pyramids of  $\text{CaN}_5$  (Fig. 1b) while the nitrogen atoms are coordinated by five Ca and one Ni atom forming layers of edge-sharing  $\text{NCa}_5\text{Ni}$  octahedra. In solid state chemistry, two-fold coordination of transition metals has for example been observed in  $\text{Na}_2\text{HgO}_2$ -type compounds such as  $\text{M}_2\text{NiO}_2$  ( $M = \text{K, Rb and Cs}$ ) and  $\text{A}_2\text{ZnN}_2$  ( $A = \text{Ca, Sr, Ba}$ ), and

nitridometallates of Co, Ni and Cu with either linear chains, kinked chains, or  $[\text{MN}_2]$ -dumbbells such as AMN-type compounds,  $(\text{BaCa}_4[\text{MN}_2]_2)$  ( $M = \text{Co, Cu}$ ) and  $\text{Sr}_{39}\text{Co}_{12}\text{N}_{31}$ .<sup>34–40</sup> The interatomic distances in the  $\text{CaN}_5$  square pyramid (Fig. 1c) are equal in the equatorial plane and both Ca–N distances (Fig. 1d) are in the range observed in similar compounds like  $\text{CaNiN}$ ,  $\text{Ca}_2\text{ZnN}_2$ ,  $\text{Ca}_2\text{FeN}_2$ ,  $\text{Ca}_4\text{FeN}_4$ ,  $\text{Ca}_5\text{Co}_2\text{N}_4$ , and  $\text{Ca}_3\text{N}_2$  ( $d_{\text{Ca–N}} = 2.40\text{--}2.82$  Å).<sup>13,32,36,41–43</sup> The Ni–N distance observed in  $\text{Ca}_2\text{NiN}_2$  is smaller than in compounds containing infinite N–Ni–N chains like  $\text{CaNi}^{\text{I}}\text{N}$  ( $d_{\text{Ni–N}} = 1.792(1)$  Å) and  $\text{BaNi}^{\text{I}}\text{N}$  ( $d_{\text{Ni–N}} = 1.8281(1)$ ,  $1.781(1)$  Å), which is probably owed to the higher oxidation state of Ni and the terminal Ni–N bonds.<sup>13,17</sup>

Bond valence sum (BVS) calculations were performed for Ca and Ni for a coordination sphere of 4 Å using bond valence parameters reported by O’Keeffe (Table S3, ESI†). The bond valence sum for Ni  $V_{\text{Ni,N}} = 2.03$  corroborates the presence of  $\text{Ni}^{\text{II}}$ , while the bond valence sum for Ca is slightly lower with  $V_{\text{Ca–N}} = 1.80$ .<sup>44</sup> This is probably owed to the covalent bonding in nitrides and metal–metal interactions and has also been observed in related compounds such as  $\text{CaGaN}$  ( $V_{\text{Ga–N}} = 0.9$ ),  $\text{Ca}_4\text{FeN}_4$  ( $V_{\text{Ca–N}} = 1.85, 1.65$ ), and the isotopic  $\text{Ca}_2\text{ZnN}_2$  ( $V_{\text{Ca–N}} = 1.82$ ).<sup>32,35,45,46</sup>

Magnetic susceptibility measurements (Fig. 2) carried out at 30 kOe in the temperature range from 2.5 to 300 K showed a broad maximum at *ca.* 200 K and a decrease towards lower temperatures. The higher temperature region of the susceptibility is indicative of short-range low-dimensional antiferromagnetic spin interactions, which also has been observed in related nitridometallates such as  $\text{Ca}_3\text{CrN}_3$  and  $\text{Ba}_4\text{Mn}_3\text{N}_6$ .<sup>23,47</sup> The derivative  $d\chi/dT$  (Fig. S2, ESI†) shows a maximum at  $T_{\text{N}} = 74$  K indicating the possible onset of long-range magnetic ordering. Neutron diffraction data will be needed to confirm this.

The susceptibility data were fit according to  $\chi_{\text{mol}} = \chi_{\text{C}} + \chi_{\text{BF}}$  with a Bonner–Fisher-type function  $\chi_{\text{BF}}$  and a Curie function  $\chi_{\text{C}}$  to account for an impurity producing a Curie tail at low temperatures (see methods for details, ESI†).<sup>48</sup> The resulting fit (Fig. 2) follows the data well, with a deviation below  $\sim 75$  K close to the maximum in  $d\chi/dT$  at 74 K (Fig. S2, ESI†). The fitted

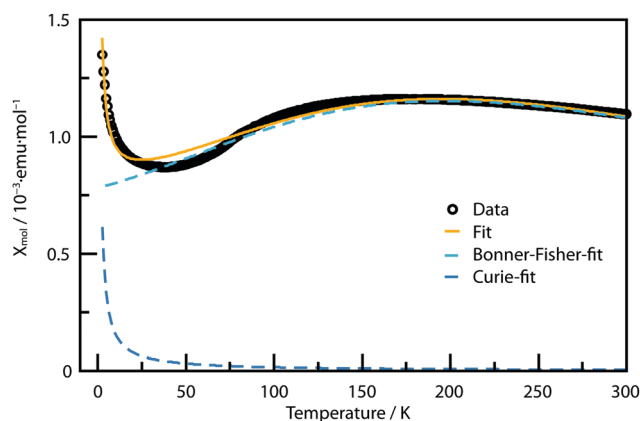


**Fig. 2** Magnetic molar susceptibility of  $\text{Ca}_2\text{NiN}_2$  measured in a field of 30 kOe with black circles as datapoints and combined Bonner–Fisher and Curie-tail fit as orange line.



paramagnetic moment of  $\mu_{\text{eff}} = 2.19 \mu_{\text{B}}$  is reduced from the ideal  $S = 1$  spin-only value of  $2.83 \mu_{\text{B}}$ , most likely due to mixing with excited states through spin-orbit coupling. The fitted exchange coupling of  $J = -157 \text{ K}$  confirms strong antiferromagnetic coupling within the  $ab$ -planes. Both the  $\mu_{\text{eff}}$  and  $J$  values are consistent with localised  $\text{Ni}^{2+}$  moment behavior. The impurity phase has an effective moment of  $0.11 \mu_{\text{B}}$ , equivalent to 0.4% of a  $S = \frac{1}{2}$  byproduct, which is below the detection limit of powder diffraction. The low-dimensional magnetic behavior reflects the arrangement of Ni-atoms in square nets with interatomic distances of  $d_{\text{Ni-Ni}} = 3.572(1) \text{ \AA}$ , which are separated by layers of  $\text{CaN}_3$  square-pyramids. Field-dependent magnetization data at 300 and 2.5 K (Fig. S2, ESI†) shows a linear dependence in accordance with paramagnetic or antiferromagnetic behavior.

The high-temperature behavior of  $\text{Ca}_2\text{NiN}_2$  was investigated with temperature-dependent powder X-ray diffraction (Fig. 3) and reveals Vegard-type behavior of the lattice parameters up to  $600 \text{ }^\circ\text{C}$  with thermal expansion coefficients of  $\alpha_a = 1.8(1) \times 10^{-5} \text{ K}^{-1}$  and  $\alpha_c = 7.1(6) \times 10^{-6} \text{ K}^{-1}$ . The larger value of  $\alpha_a$  reflects greater amplitudes of thermal vibration perpendicular to the  $\text{NiN}_2$  dumbbells which are aligned in the  $c$ -direction. Above this temperature  $\text{Ca}_2\text{NiN}_2$  starts to decompose through elimination of  $\frac{1}{2} \text{N}_2$  and 1 Ca per formula unit resulting in crystalline  $\text{CaNiN}$ .<sup>13</sup>  $\text{Ca/Ca}_3\text{N}_2$  could not unambiguously be identified in the powder patterns and might also be amorphous. The decomposition was monitored through phase fractions, which show gradual decomposition over a wider temperature range, which might be owed to the relatively fast data collection of 30 min per step. At  $960 \text{ }^\circ\text{C}$  the capillary presumably broke as  $\text{CaNiN}$ , which was reported to be stable up to  $1100 \text{ }^\circ\text{C}$ , decomposed into  $\text{CaO}$  and metallic  $\text{Ni}$ .<sup>6</sup>

In conclusion, the preparation of  $\text{Ca}_2\text{NiN}_2$  with Ni in oxidation state +II, which is very unusual for nitridometallates, is demonstrated through the azide-mediated nitridation of metallic Ni under high-pressure conditions.  $\text{Ca}_2\text{NiN}_2$  crystallizes in the  $\text{Na}_2\text{HgO}_2$  structure type with linear coordination of Ni. While in molecular chemistry low metal coordination environments are stabilized through sterically demanding ligands, the stabilization here is probably due to covalent Ni-N multiple bonding and consequent short Ni-N bond distances and the electron inductive effect of the surrounding  $\text{Ca}^{2+}$  matrix.<sup>49</sup> The observation of a susceptibility maximum consistent with low-dimensional antiferromagnetic ordering of  $\text{Ni}^{2+}$  spins in  $\text{Ca}_2\text{NiN}_2$ , whereas metallic  $\text{CaNiN}$  has a temperature-independent Pauli susceptibility, suggests that  $\text{Ca}_2\text{NiN}_2$  is non-metallic but further measurements will be required to confirm this. Temperature-dependent powder X-ray diffraction shows that  $\text{Ca}_2\text{NiN}_2$  is stable up to  $600 \text{ }^\circ\text{C}$  before decomposing to  $\text{CaNiN}$ , which when compared to the synthesis temperature of  $900 \text{ }^\circ\text{C}$  indicates the stabilizing influence of the high-pressure conditions. Stability estimates are particularly important for efficient planning of syntheses of compounds of noble metals like Ni and Cu, and our results highlight that nitrogen-rich compounds require very stringent temperature control which necessitates synthesis under a high nitrogen chemical potential. Discovery of  $\text{Ca}_2\text{NiN}_2$

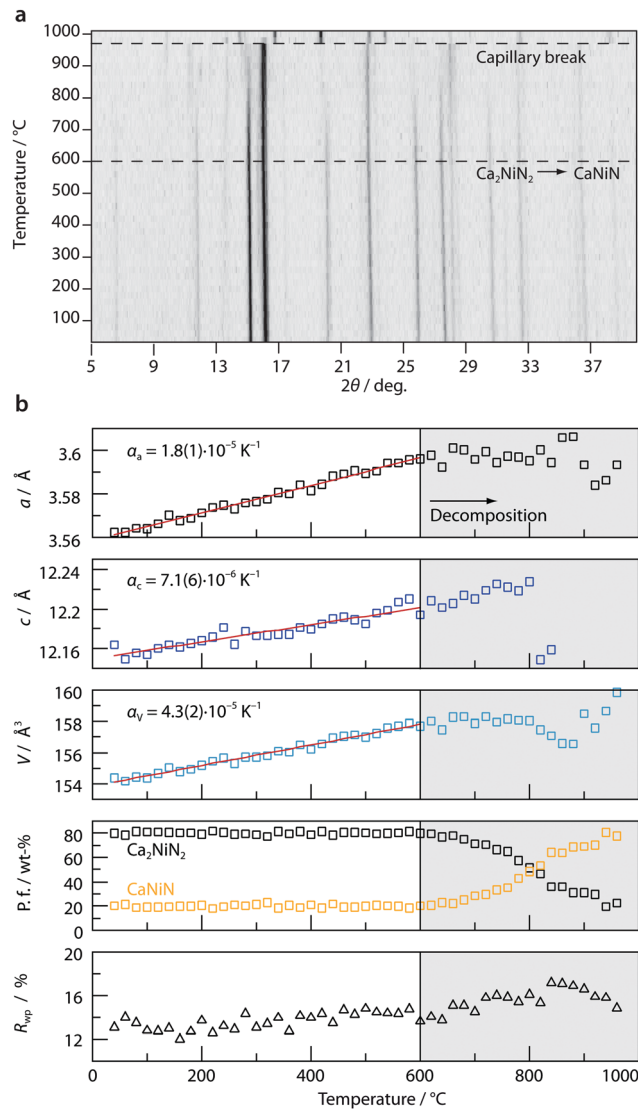


**Fig. 3** (a) Temperature-dependent PXR D of a  $\text{Ca}_2\text{NiN}_2$  sample containing a 20 wt% impurity of  $\text{CaNiN}$ . Dashed lines indicate decomposition onset and capillary break. (b) Results of the Rietveld analysis up to  $960 \text{ }^\circ\text{C}$  showing evolution of lattice parameters  $a$ ,  $c$ , and volume  $V$  with temperature as well as the decomposition of  $\text{Ca}_2\text{NiN}_2$  into  $\text{CaNiN}$  as a function of phase fraction (p. f.). Linear regressions (red lines) were used to extract thermal expansion parameters of  $\text{Ca}_2\text{NiN}_2$ . The fit quality is monitored through  $R_{\text{wp}}$ , which increases with temperature owed to decreasing data quality. Estimated standard deviations (ESD) of individual datapoints are too small to be displayed.

indicates that a new class of late transition metal nitrides can be synthesised, and like oxo-nickelates and -cuprates, they may have interesting correlated electron properties in proximity to a metal-insulator boundary, as illustrated by the recent discovery of superconductivity in infinite-layer nickelates  $\text{LnNiO}_2$ .<sup>50</sup>

## Conflicts of interest

There are no conflicts to declare.



## Notes and references

- R. Niewa and F. J. DiSalvo, *Chem. Mater.*, 1998, **10**, 2733.
- H. Yamane and F. J. DiSalvo, *Prog. Solid State Chem.*, 2018, **51**, 27.
- N. Tapia-Ruiz, M. Segalés and D. H. Gregory, *Coord. Chem. Rev.*, 2013, **257**, 1978.
- J. M. Cameron, R. W. Hughes, Y. Zhao and D. H. Gregory, *Chem. Soc. Rev.*, 2011, **40**, 4099.
- R. Niewa and H. Jacobs, *Chem. Rev.*, 1996, **96**, 2053.
- F. J. DiSalvo and S. J. Clarke, *Curr. Opin. Solid State Mater. Sci.*, 1996, **2**, 241.
- F. J. DiSalvo, *Science*, 1990, **247**, 649.
- D. R. Glasson and S. A. A. Jayaweera, *J. Appl. Chem.*, 1968, **18**, 65.
- W. Sun, A. Holder, B. Orvañanos, E. Arca, A. Zakutayev, S. Lany and G. Ceder, *Chem. Mater.*, 2017, **29**, 6936.
- A. Salamat, A. L. Hector, P. Kroll and P. F. McMillan, *Coord. Chem. Rev.*, 2013, **257**, 2063.
- P. P. Power, *Chem. Rev.*, 2012, **112**, 3482–3507.
- V. Vreeken, M. A. Siegler, B. de Bruin, J. N. H. Reek, M. Lutz and J. I. van der Vlugt, *Angew. Chem., Int. Ed.*, 2015, **54**, 7055 (*Angew. Chem.*, 2015, **127**, 7161–7165).
- M. Y. Chern and F. J. DiSalvo, *J. Solid State Chem.*, 1990, **88**, 459.
- T. Yamamoto, S. Kikkawa and F. Kanamaru, *J. Solid State Chem.*, 1995, **115**, 353.
- A. Gudat, R. Kniep and A. Rabenau, *Z. Anorg. Allg. Chem.*, 1991, **597**, 61.
- A. Mehta, P. Höhn, W. Schnelle, V. Petzold, H. Rosner, U. Burkhardt and R. Kniep, *Chem. – Eur. J.*, 2006, **12**, 1667.
- A. Gudat, S. Haag, R. Kniep and A. Rabenau, *J. Less-Common Met.*, 1990, **159**, L29.
- C. H. Hu, Y. Yang and Z. Z. Zhu, *Solid State Commun.*, 2010, **150**, 669.
- G. R. Kowach, N. E. Brese, U. M. Bolle, C. J. Warren and F. J. DiSalvo, *J. Solid State Chem.*, 2000, **154**, 542.
- P. Höhn, M. Armbrüster, G. Auffermann, U. Burkhardt, F. Haarmann, A. Mehta and R. Kniep, *Z. Anorg. Allg. Chem.*, 2006, **632**, 2129.
- P. Chanhom, K. E. Fritz, L. A. Burton, J. Kloppenburg, Y. Filinchuk, A. Senyshyn, M. Wang, Z. Feng, N. Insin, J. Suntivich and G. Hautier, *J. Am. Chem. Soc.*, 2019, **141**, 10595.
- M. Yang, A. Zakutayev, J. Vidal, X. Zhang, D. S. Ginley and F. J. DiSalvo, *Energy Environ. Sci.*, 2013, **6**, 2994.
- D. A. Vennos, M. E. Badding and F. J. DiSalvo, *Inorg. Chem.*, 1990, **29**, 4059.
- R. Marchand and V. Lemarchand, *J. Less-Common Met.*, 1981, **80**, 157.
- A. Zakutayev, *J. Mater. Chem. A*, 2016, **4**, 6742.
- W. Sun, C. J. Bartel, E. Arca, S. R. Bauers, B. Matthews, B. Orvañanos, B.-R. Chen, M. F. Toney, L. T. Schelhas, W. Tumas, J. Tate, A. Zakutayev, S. Lany, A. M. Holder and G. Ceder, *Nat. Mater.*, 2019, **18**, 732.
- K. Niwa, R. Fukui, T. Terabe, T. Kawada, D. Kato, T. Sasaki, K. Soda and M. Hasegawa, *Eur. J. Inorg. Chem.*, 2019, 3753–3757.
- J. C. Crowhurst, *Science*, 2006, **311**, 1275.
- M. Bykov, E. Bykova, G. Aprilis, K. Glazyrin, E. Koemets, I. Chuvashova, I. Kupenko, C. McCammon, M. Mezouar, V. Prakapenka, H.-P. Liermann, F. Tasnádi, A. V. Ponomareva, I. A. Abrikosov, N. Dubrovinskaia and L. Dubrovinsky, *Nat. Commun.*, 2018, **9**, 2756.
- D. Laniel, G. Weck, G. Gaiffe, G. Garbarino and P. Loubeyre, *J. Phys. Chem. Lett.*, 2018, **9**, 1600.
- G. Serghiou, G. Ji, N. Odling, H. J. Reichmann, J.-P. Morniroli, R. Boehler, D. J. Frost, J. P. Wright and B. Wunder, *Angew. Chem., Int. Ed.*, 2015, **54**, 15109 (*Angew. Chem.*, 2015, **127**, 15324).
- S. D. Kloss, A. Haffner, P. Manuel, M. Goto, Y. Shimakawa and J. P. Attfield, *Nat. Commun.*, 2021, **12**, 571.
- M. Bykov, K. R. Tasca, I. G. Batyrev, D. Smith, K. Glazyrin, S. Chariton, M. Mahmood and A. F. Goncharov, *Inorg. Chem.*, 2020, **59**, 14819.
- T. Yamamoto, S. Kikkawa and F. Kanamaru, *Solid State Ionics*, 1993, **63–65**, 148.
- H. Rieck and R. Hoppe, *Z. Anorg. Allg. Chem.*, 1973, **400**, 311.
- M. Y. Chern and F. J. DiSalvo, *J. Solid State Chem.*, 1990, **533**, 528.
- H. Yamane and F. J. DiSalvo, *J. Solid State Chem.*, 1995, **119**, 375.
- J. K. Bendyna, P. Höhn, Y. Prots and R. Kniep, *Z. Kristallogr. - New Cryst. Struct.*, 2007, **222**, 484.
- G. R. Kowach, H. Y. Lin and F. J. DiSalvo, *J. Solid State Chem.*, 1998, **9**, 1–9.
- R. Niewa and F. J. DiSalvo, *J. Alloys Compd.*, 1998, **279**, 153–160.
- P. Höhn and R. Kniep, *Z. Naturforsch.*, 1992, **47b**, 477–481.
- J. K. Bendyna, P. Höhn and R. Kniep, *Z. Kristallogr. - New Cryst. Struct.*, 2007, **222**, 165.
- Y. Laurent, J. Lang and M. T. Le Bihan, *Acta Crystallogr., Sect. B: Struct. Crystallogr. Cryst. Chem.*, 1968, **24**, 494.
- N. E. Brese and M. O'Keeffe, *Acta Crystallogr., Sect. B: Struct. Sci.*, 1991, **47**, 192.
- N. E. Brese and M. O'Keeffe, *Crystal chemistry of inorganic nitrides in Complexes, Clusters and Crystal Chemistry*, Springer-Verlag, Berlin/Heidelberg, 2006, p. 307.
- D. H. Gregory, *J. Chem. Soc., Dalton Trans.*, 1999, 259.
- A. Ovchinnikov, M. Bobnar, Y. Prots, W. Schnelle, P. Höhn and Y. Grin, *Crystals*, 2018, **8**, 235.
- M. E. Fisher, *Am. J. Phys.*, 1964, **32**, 343.
- J. Etourneau, J. Portier and F. Ménil, *J. Alloys Compd.*, 1992, **188**, 1.
- D. Li, K. Lee, B. Y. Wang, M. Osada, S. Crossley, H. R. Lee, Y. Cui, Y. Hikita and H. Y. Hwang, *Nature*, 2019, **572**, 624.

